Dynamic Modeling of Elastic Tendon Actuators with Tendon Slackening

Thomas Lens, Jérôme Kirchhoff and Oskar von Stryk

Abstract—This paper presents a new, detailed dynamics model of a novel type of actuators based on tendons with integrated springs that allows for offline adjustment of the stiffness characteristics. Like other cable or belt actuators, the elastic tendon actuator allows to radically reduce the link inertia by placing the motors near the robot base. But by additionally integrating springs in the tendons, the motor and the joint are elastically decoupled, which increases the lifespan of the tendons and the safety of the actuator. A detailed mathematical model of the actuator is derived taking tendon slackening effects into consideration. The result is a degressive stiffness curve that depends on the pretension force of the integrated tendon springs. The derived model is validated against static and dynamic experimental measurement data of a robot arm equipped with elastic tendon actuators.

I. INTRODUCTION

Applications with close physical human-robot interaction increase the need for safe robot arms. Introducing elasticity can increase safety when using geared motors because of the decoupling of motor and joint [1]–[4]. The degree of elasticity does not necessarily have to be high. In [5] it has been shown that even the elasticity introduced by Harmonic Drives can be sufficient to actively decouple the motor from the joint side in case of a collision. Elasticity can be realized by using inherently compliant actuators, such as artificial pneumatic muscles [6], [7] or by using elastic elements in series with standard geared motors [1], [8]. Additional actuators can be used to adapt stiffness or damping [9]–[11], or to combine actuators with complementary features, such as electromotors and pneumatic actuators [12].

The use of cables in robotic arms can also contribute to safety by allowing to place the motors away from the actuated joints to previous links in the kinematic chain and therefore reducing the link weights [13], [14]. As a drawback, special care has to be taken in the design process regarding the lifespan of the tendons [15].

The actuation approach of the BioRob arm as shown in Figure 12 is inspired by the human elastic muscle tendon apparatus and aims at combining the robust behavior of standard electrical motors with the safety characteristics of elasticity in the drivetrain and a radical lightweight design by using tendons to actuate the robot joints. When using tendons spanning multiple joints, additional friction is introduced. However, this comes also with several advantages. By using tendons, the motors can be placed near the base, thus reducing the robot arm's inertia. As an alternative, they can even be

The authors are with the Simulation, Optimization and Robotics Group, Computer Science, Technische Universität Darmstadt, Germany [lens,kirchhoff,stryk]@sim.tu-darmstadt.de

used as a counterbalance for the weight of the links. The reduction of mass and inertia allows to use smaller and less heavy motors and gears. In addition, by using elasticity in the tendons, the reflected rotor inertia and friction are dynamically decoupled from the link side, reducing shocks on the gearbox as well as on the environment in case of a collision. This increases safety and the durability of the tendons.

In this paper, a detailed mathematical model for a single joint elastic tendon actuator, as displayed in Figure 1, will be derived. The specific characteristics of this actuator will be analyzed, such as the case of static tendon slacking, the characteristic stiffness and damping curves, and the role of prestretching for shaping the characteristic curves.

II. SINGLE JOINT ELASTIC TENDON ACTUATOR MODEL

For the derivation of the single elastic tendon actuator it is assumed that the elastic elements integrated in the tendons can be approximated as massless springs. This is a valid assumption if the mass of the springs is small compared to the effective mass of the motor and gearbox inertia and the effective mass of the joint pulley and attached link. For the motors, this is especially true when using gearboxes with high reduction ratios. The effective mass of the link is normally also higher by at least one magnitude.

Only in case of a very lightweight last link without attached further links and without end-effector or load, the spring mass may not be negligible compared to the effective link mass. In this case the spring and link with low joint damping can behave as a two-mass oscillator. Excited at the resonance frequency by minimal motor motions, the spring and link can easily start oscillating. The constellation of two-mass oscillator driven by the motor is highly undesirable and unfavorable for control and should be avoided by choosing a spring with a mass at least a magnitude smaller than the effective link mass.

A. Kinematics

As according to Figure 2, the lengthening x_i of the springs depends on the radius R of the joint pulley, the radius r of the motor pulley, the angular joint position q, and the angular motor position with respect to the elastic actuator ${}^e\theta$

$$x_1 = -R\,q + r\,{}^e\theta \tag{1}$$

$$x_2 = R\,q - r\,{}^e\theta = -x_1 \tag{2}$$

Because of the kinematic constraint of a constant tendon length, the displacement x_1 of the upper spring equals the negative displacement $-x_2$ of the lower spring. The tendons
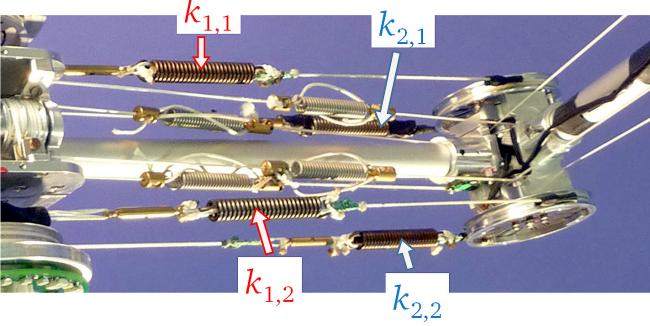
Figure 1. Third joint connecting the second and third link of the BioRob-X4 arm actuated by two parallel elastic tendon actuators. Both actuators have an upper spring with stiffness $k_{1,i}$ and a lower spring with stiffness $k_{2,i}$.
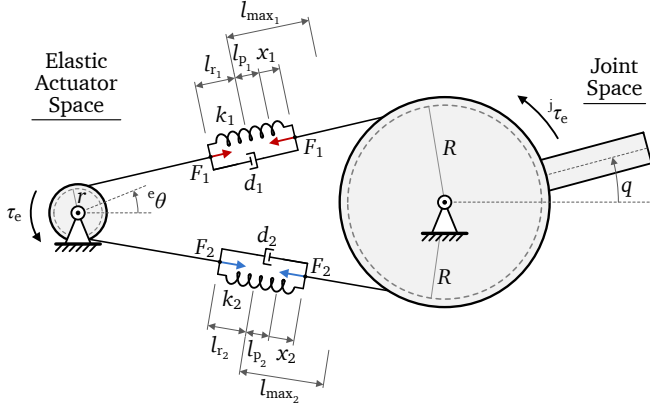

Figure 2. Model of the elastic transmission with parameters motor pulley radius r, joint pulley radius R, spring rest length l_r, spring prestretched deflection l_p, maximum spring deflection l_{max}, and state variables angular joint position q, angular motor position with respect to the elastic actuator $^e\theta$, elastic actuator torque τ_e, elastic actuator joint torque $^j\tau_e$, spring force F, and spring deflection x with respect to prestretched length. The indices 1 and 2 stand for the upper and the lower spring, respectively.

are made of prestretched, high-performance polyethylene and can be regarded as stiff compared to the springs.

B. Elastic Pulley Torques

The force to displacement characteristic curve of the springs is modeled as ideally viscoelastic. The force F_i exerted by the stretched springs depends on the prestretched length l_{p_i}, the spring stiffness k_i and damping d_i and the elongation x_i

$$F_i = k_i \left(l_{p_i} + x_i\right) + d_i \dot{x}_i \tag{3}$$

and contains the prestretching force F_p

$$F_p = k_i l_{p_i} , \tag{4}$$

which prevents slack in the cables. In the equilibrium position with $x_i = 0$ and $\dot{x}_i = 0$ both spring forces equal the prestretching force, yielding the ratio of the prestretching lengths l_{p_i}

$$\frac{l_{p,1}}{l_{p,2}} = \frac{k_2}{k_1} \tag{5}$$

Table I
STATE TRANSFORMATIONS BETWEEN THE ELASTIC ACTUATOR STATE SPACE AND THE JOINT STATE SPACE WITH TRANSMISSION RATIO $n_t = \frac{R}{r}$.

State	Elastic Actuator	Joint
Elastic actuator torque	$\tau_e = \frac{1}{n_t}\,^j\tau_e$	$^j\tau_e = n_t\,\tau_e$
Motor position	$^e\theta = n_t\,^j\theta$	$^j\theta = \frac{1}{n_t}\,^e\theta$
Joint position	$^e q = n_t\,q$	$q = \frac{1}{n_t}\,^e q$

The forces F_i acting on the pulleys with radius R on the joint side and radius r on the motor side cannot become negative, as the tendons only transfer pulling forces. Cable sagging occurs for spring displacement smaller than the prestretched spring length, i.e. $x_i < l_{p_i}$, which is referred to in this paper as *static tendon slack*. The resulting torque on the joint produced by the elastic pulley actuation can be expressed using the step function σ

$$\sigma(x) = \begin{cases} 0 & : & x < 0 \\ 1 & : & x \geq 0 \end{cases} \tag{6}$$

as

$$^j\tau_e = R\,F_1\,\sigma(F_1) - R\,F_2\,\sigma(F_2) , \tag{7}$$

whereas the elastic pulley torque at the motor side yields

$$\tau_e = r\,F_1\,\sigma(F_1) - r\,F_2\,\sigma(F_2) \tag{8}$$

C. Definition of Reflected Variables

As can be seen from Equations (7) and (8), a transmission ratio n_t can be defined to reflect the elastic torque τ_e from the motor side to the joint side

$$n_t = \frac{^j\tau_e}{\tau_e} = \frac{R}{r} , \tag{9}$$

which, from Equations (1) and (2), can also be used to reflect the motor position $^e\theta$ through the elasticity to the joint side

$$\frac{1}{n_t} = \frac{^j\theta}{^e\theta} = \frac{r}{R} \tag{10}$$

With the transmission ratio, the kinematics Equations (1) and (2) can be expressed either with respect to the joint state space

$$x_1 = -R\left(q - \,^j\theta\right) = -x_2 \tag{11}$$

or with respect to the elastic actuator state space

$$x_1 = -r\left(^e q - \,^e\theta\right) = -x_2 \tag{12}$$

The reflected motor position $^j\theta$ therefore equals the joint position q if the elastic actuator is in equilibrium position with $x_i = 0$ and $\tau_e = 0$. Table I summarizes the defined state transformations.
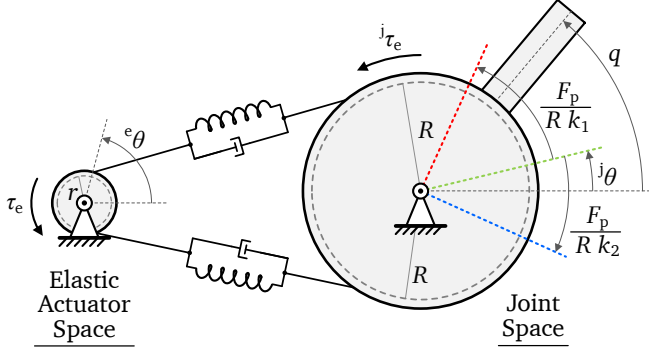
Figure 3. Model of the elastic tendon actuator with reflected variables. The motor position with respect to the join side $^{j}\theta$ marks the equilibrium position of the joint position q. The area without tendon slack is marked by joint angles between the red and blue line.
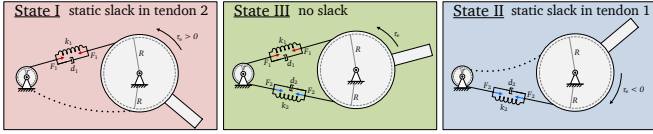

Figure 4. Definition of static tendon slack states of the elastic tendon actuator. Static slack in the tendons (indicated by dashed lines) occurs in case of large joint deflections. State I describes static slack in the lower tendon (with index 2), State II static slack in the upper tendon (with index 1), and State III is the normal operation mode without slack.

D. Static Tendon Slack and Maximum Deflection

As described in (7) and (8), slack in a tendon can be caused by the displacement $x_i + l_{p_i} < 0$. Figure 4 lists the possible states of a single joint elastic tendon actuator with respect to tendon slack.

Static slack in the lower tendon occurs if the elongation of the spring in that tendon becomes negative. This yields the constraint for the angular displacement of the joint position q with respect to the reflected motor position $^{j}\theta$

$$l_{p2} + x_2 \leq 0 \quad \Rightarrow \quad (q - ^{j}\theta) \leq -\frac{F_p}{R\,k_2} \tag{13}$$

The constraint for the upper side is calculated respectively and static tension in both tendons is therefore maintained for the angular joint displacement range

$$-\frac{F_p}{R\,k_2} \leq (q - ^{j}\theta) \leq \frac{F_p}{R\,k_1} \tag{14}$$

The maximum joint deflection is determined by the maximum spring extension $l_{\max_i}$

$$l_{\max_i} \geq l_{p_i} + x_i \tag{15}$$

yielding the joint angle constraint

$$-\frac{l_{\max_1}}{R} - \frac{F_p}{k_1 R} \leq (q - ^{j}\theta) \leq -\frac{l_{\max_2}}{R} - \frac{F_p}{k_2 R} \tag{16}$$

E. Characteristic Stiffness and Damping Curves

Figure 4 visualizes the elastic tendon actuator states that were derived in the previous section. In this section the output torque function of these states are derived.
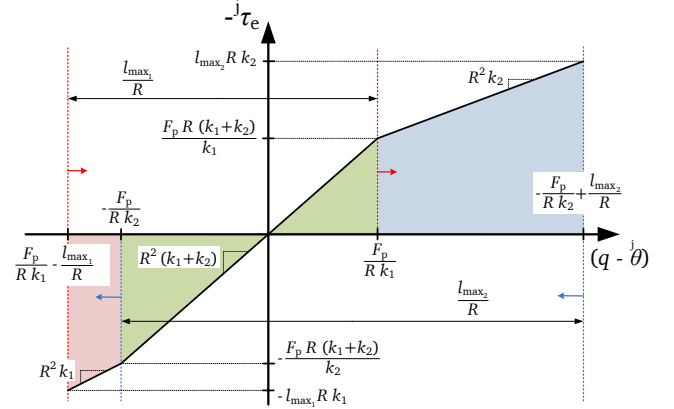

Figure 5. Characteristic stiffness curve with respect to the joint side. Example for asymmetric configuration with a stiffer spring on the upper side $k_1 = 1.33\,k_2$ with maximum deflection $l_{\max_1} = 0.67\,l_{\max_2}$.

1) State I: With dynamic or static slack in the lower tendon (index 2), the elastic torque is generated only by the taut upper tendon (index 1):

$$^{j}\tau_{e_I} = R\,(F_p + k_1\,x_1 + d_1\,\dot{x}_1) \tag{17}$$

$$= R\,F_p - k_1\,R^2\left(q - ^{j}\theta\right) - d_1\,R^2\left(\dot{q} - ^{j}\dot{\theta}\right) \tag{18}$$

The actuator output stiffness and damping can be obtained by derivation with regard to the joint deflection and the joint deflection velocity

$$^{j}k_{e_I} = -\frac{\partial \tau_{e_I}}{\partial(q - ^{j}\theta)} = R^2\,k_1 \tag{19}$$

$$^{j}d_{e_I} = -\frac{\partial \tau_{e_I}}{\partial(\dot{q} - ^{j}\dot{\theta})} = R^2\,d_1 \tag{20}$$

2) State II: Equivalent to State I, with transposed indices: the elastic torque is generated only by the taut lower tendon (index 2):

$$^{j}\tau_{e_{II}} = -R\,(F_p + k_2\,x_2 + d_2\,\dot{x}_2) \tag{21}$$

$$= -R\,F_p - k_2\,R^2\left(q - ^{j}\theta\right) - d_2\,R^2\left(\dot{q} - ^{j}\dot{\theta}\right) \tag{22}$$

with stiffness and damping

$$^{j}k_{e_{II}} = R^2\,k_2 \quad , \quad ^{j}d_{e_{II}} = R^2\,d_2 \tag{23}$$

3) State III: Without slack, both tendons contribute to the elastic torque:

$$^{j}\tau_{e_{III}} = -R^2\,(k_1 + k_2)\left(q - ^{j}\theta\right)$$
$$\qquad\qquad - R^2\,(d_1 + d_2)\left(\dot{q} - ^{j}\dot{\theta}\right) \tag{24}$$

with stiffness and damping

$$^{j}k_{e_{III}} = R^2\,(k_1 + k_2) \quad , \quad ^{j}d_{e_{III}} = R^2\,(d_1 + d_2) \tag{25}$$

The resulting steady state characteristic stiffness curve is plotted in Figure 5. The shifting direction of the area borders for increasing prestretching force F_p are indicated
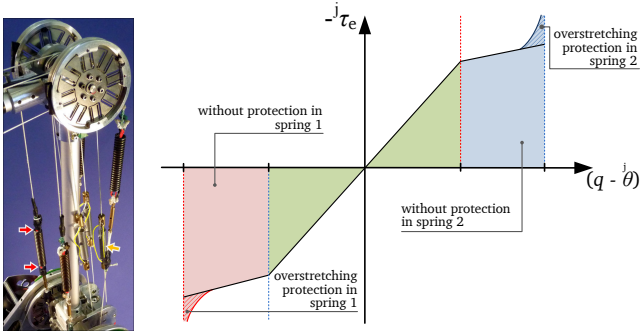
Figure 6. Symmetric spring configuration with protection against over-stretching causing a progressive curve. Possible hardware implementations for the protective elements are displayed in the left picture. Protective strings guided within the springs are marked in red, strings on the outside of the springs are marked in yellow.
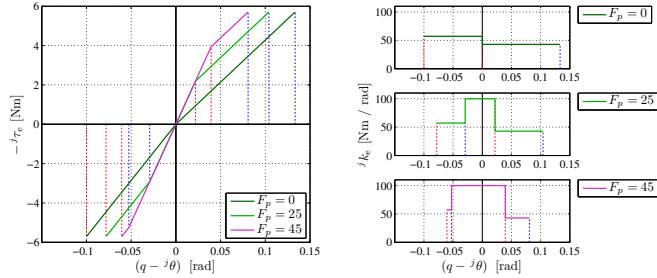

Figure 7. Effect of prestretching on the characteristic stiffness curve with respect to the joint side. Example for asymmetric configuration with $k_1 = 22.820\,\text{kN/m}$, $k_2 = 0.75\,k_1$, $l_{\max_1} = 5\,\text{mm}$, $l_{\max_2} = 1.33\,l_{\max_1}$, $R = 5\,\text{cm}$. The maximum torque remains constant, whereas the maximum joint deflection decreases for increasing pretension force F_p.

with arrows. The area with slack in the upper spring is marked in red, as well as the borders with a dependence on parameters of the upper spring. Respectively, the area and borders that are marked in blue are related to the lower spring.

III. DESIGN AND DIMENSIONING GUIDELINES

A. Guidelines for Choosing the Spring Stiffness

If the stiffnesses of the upper and lower spring differ, an asymmetric stiffness curve configuration results. Examples for a stiffer upper spring are shown in Figure 5 and Figure 7.

These configurations can be useful for operation where the direction of gravity is predefined. The asymmetric stiffness curve exhibits a larger high stiffness area for negative joint deflection angles and therefore compensates the joint angle equilibrium shift caused by gravitational forces.

B. Guidelines for Setting the Prestretching Force

The high stiffness area (both springs are loaded and both tendons taut) can be increased by increasing the prestretching force F_p. Figure 5 displays the boundaries of the areas with combined and single stiffness. The arrows indicate the shifting direction of the boundaries in case F_p is increased. The maximum allowed prestretching force is represented by
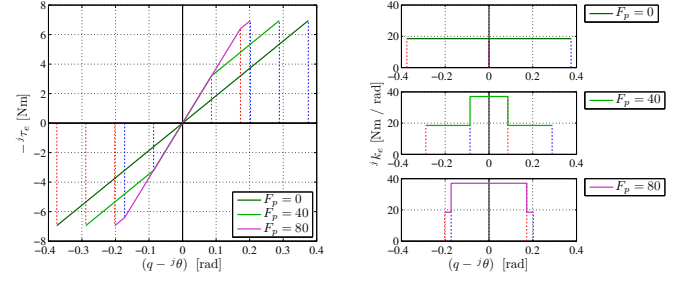

Figure 8. Effect of prestretching on the characteristic stiffness curve with respect to the joint side. Example for symmetric configuration with $k_i = 11.580\,\text{kN/m}$, $l_{\max_i} = 15\,\text{mm}$, $R = 4\,\text{cm}$. The maximum torque remains constant, whereas the maximum joint deflection decreases for increasing pretension force F_p.

the outer boundaries of the characteristic curve:

$$\frac{F_\mathrm{p}}{R\,k_i} = \frac{l_{\max_i}}{R} \,, \tag{26}$$

which yields

$$F_\mathrm{p,max} = \min_{i=\{1,2\}}\left(l_{\max_i}\,k_i\right) \tag{27}$$

A more reasonable upper limit, however, is given by maximizing the high stiffness area. Maximizing the high stiffness area for negative deflections yields

$$\frac{F_\mathrm{p}}{R\,k_1} - \frac{l_{\max_1}}{R} = -\frac{F_\mathrm{p}}{R\,k_2} \,, \tag{28}$$

whereas maximizing the high stiffness area for positive deflections yields

$$-\frac{F_\mathrm{p}}{R\,k_2} + \frac{l_{\max_2}}{R} = \frac{F_\mathrm{p}}{R\,k_1} \tag{29}$$

The combined maximum limit is therefore given by

$$F_\mathrm{p,max} = \min_{i=\{1,2\}}\left(l_{\max_i}\left(\frac{1}{k_1} + \frac{1}{k_2}\right)^{-1}\right) \tag{30}$$

For springs with equal maximum stretching length $l_{\max}$, the maximum pretention force can be therefore chosen as:

$$F_\mathrm{p} = l_{\max}\left(\frac{1}{k_1} + \frac{1}{k_2}\right)^{-1} \,, \tag{31}$$

which maximizes the high stiffness area in both positive and negative direction of deflection. It should be ensured that the mechanical joint construction can bear the given prestretching forces as well as dynamical and external forces.

C. Guidelines for Increasing the Maximum Output Torque

The maximum output torque can be increased by using springs with a higher maximum force $F_{\max_i}$ and an appropriate maximum deflection $l_{\max_i}$

$$F_{\max_i} = l_{\max_i}\,k_i \tag{32}$$

It must be noted, however, that heavier springs increase the danger of undesired oscillations of the spring mass.

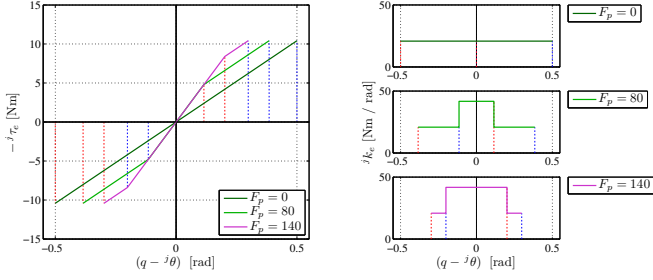Figure 9. Characteristic stiffness curve of BioRob-X4 joint 3 with two parallel elastic tendon actuators with spring stiffness $k_i = 11.580\,\mathrm{kN/m}$, maximum spring elongation $l_{\max_i} = 15\,\mathrm{mm}$, and joint pulley radius $R = 3\,\mathrm{cm}$. The resulting stiffness curves for various spring preloading forces F_p are shown.

If no stiffer spring with the desired properties is available, parallel tendons with equal springs can be used. In this case, the resulting spring stiffness is the sum of all spring stiffnesses used in parallel. Figure 1 displays the use of two parallel tendons for joint three of the BioRob-X4 arm, resulting in the combined stiffnesses

$$k_1 = k_{1,1} + k_{1,2} \tag{33}$$
$$k_2 = k_{2,1} + k_{2,2} \tag{34}$$

In addition, the use of parallel tendons is also advantageous in that it allows for a more homogeneous distribution of stress on the joint bearing.

IV. EXPERIMENTAL VALIDATION

In this section, the theoretical models derived in the previous sections are validated by comparing the models with experimental measurements from the BioRob-X4 arm. All four joints of this robot arm, as displayed in Figure 12, are driven by elastic tendon actuators [8]. The design leads to a very low overall weight of the robot arm of $4\,\mathrm{kg}$ (including power electronics), while still enabling it to carry an end-effector load of $2\,\mathrm{kg}$ without exceeding the maximum torques.

For validation of the actuator models, the joint torque over joint deflection characteristic curve of the third joint was measured and compared to the theoretical models.

The stiffness of the springs is given as $k = 11.580\,\mathrm{kN/m}$. Because two parallel cables are used, the stiffness values are added, cf. (33),

$$k_i = k_{i,1} + k_{i,1} = 23.160\,\mathrm{kN/m} \tag{35}$$

No additional damping elements are used in parallel to the springs, and the internal damping of the springs and tendons is small compared to the damping in the joints and motors. Therefore, the damping parameters of the elastic transmission are set to $d_i = 0\,\mathrm{Ns/m}$.

The border values of the stiffness curve for joint three of the BioRob-X4 arm can be calculated with the parameters $l_{\max_i} = 15\,\mathrm{mm}$, $R = 3\,\mathrm{cm}$, and a pretension force of $F_\mathrm{p} = 80\,\mathrm{N}$. The static slack boundary lies at

$$\pm(q - {}^\mathrm{j}\theta) = \frac{F_\mathrm{p}}{R\,k_i} = 0.115\,\mathrm{rad} = 6.60\,^\circ\,, \tag{36}$$
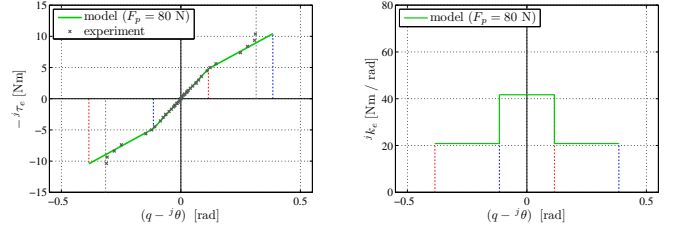

Figure 10. Experimental validation with comparison of theoretical model with measured characteristic stiffness curve of the third joint of a BioRob-X4 arm with two parallel elastic tendon actuators with spring stiffness $k_{i,j} = 11.580\,\mathrm{kN/m}$, maximum spring elongation $l_{\max_i} = 15\,\mathrm{mm}$, and joint pulley radius $R = 3\,\mathrm{cm}$.
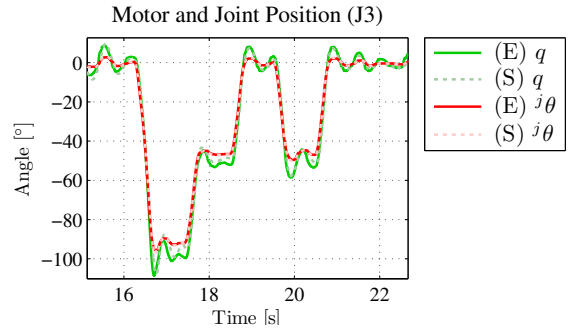

Figure 11. Experimental data (solid lines, marked with 'E') of an excitation trajectory of the third joint of a BioRob-X4 arm compared with the simulated dynamic behavior using the elastic tendon actuator model (dashed lines, marked with 'S').

and the maximum joint deflection at

$$\pm(q - {}^\mathrm{j}\theta) = -\frac{F_\mathrm{p}}{R\,k_i} + \frac{l_{\max_i}}{R} = 0.385\,\mathrm{rad} = 22.05\,^\circ \tag{37}$$

The angular stiffness and damping parameters in the state without slack (State III) are

$$k_{\mathrm{e_{III}}} = R^2\,(k_1 + k_2) = 41.69\,\mathrm{Nm/rad} \tag{38}$$

and in case of static slack (State I and II)

$$k_{\mathrm{e_I}} = R^2\,k_1 = k_{\mathrm{e_{II}}} = R^2\,k_2 = 20.8\,\mathrm{Nm/rad} \tag{39}$$

The resulting characteristic torque and stiffness curves of the BioRob-X4 elastic tendon actuator for the third joint are displayed in Figure 9 and the experimental measurement data for validation is compared to the model in Figure 10. The measured values match the derived model quite well. The deviation of the measured data at the corners of the stiffness curve is due to the use of overstretching protection in the springs, as depicted in Figure 6.

In addition to the static measurements, also a validation of the dynamic behavior of the elastic tendon actuator was conducted, as shown in Figure 11. For this experiment, the motor position was controlled according to a given excitation trajectory ${}^\mathrm{j}\theta_\mathrm{d}$ with respect to the joint side. The resulting joint trajectory q in simulation shows a good agreement with the measured experimental data.
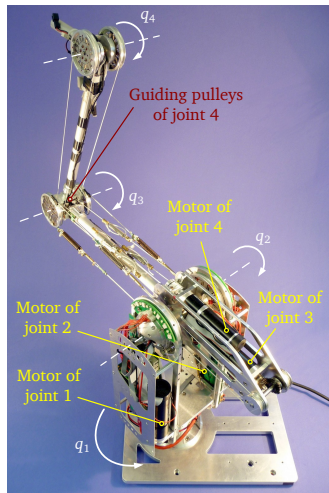
5

Figure 12. Location of the electrical DC motors in the BioRob-X4 arm with four joints driven by elastic tendon actuators.

V. Conclusion

In this paper, a novel type of actuators based on electrical DC motors and tendons with integrated springs for construction of low inertia robotic arms with high levels of mechanical safety and high acceleration and velocity properties was presented.

A detailed mathematical model of the actuator was developed and validated by comparing the theoretical models with experimental measurement data from the BioRob-X4 robot arm equipped with elastic tendon actuators, which showed good conformity of the model compared to the hardware in both the static as well as in the dynamic case.

The elastic tendon actuators can be used to construct robotic arms with more human-like properties regarding safety and speed than most current robotic arms. For example, the BioRob-X4 with elastic tendon actuators in all of its four joints can achieve end effector velocities higher than $6\,\mathrm{m/s}$ while maintaining a high level of safety [16].

Humanoids can benefit from elastic tendon actuators because this type of actuators allows an excellent mass distribution with very low links weights by placing the motors in the robot's torso. The passive compliance of the actuators and the possibility to shape the stiffness curve to an asymmetric gravity-based configuration or to a degressive behavior are very useful properties for humanoids intended for applications with close physical human-robot interaction (pHRI).

The presented actuation concept allows to drastically reduce the effective mass of robot arms by more than $90\,\%$ compared to conventional designs [17] while still allowing high relative payloads. The intrinsic mechanical actuator compliance combined with the low effective mass offer very high safety properties for humanoids robots for pHRI. In this context, the developed and validated dynamics models presented in this paper play a crucial role for dimensioning of the actuator parameters and model based control of robot arms driven by elastic tendon actuators.

References

[1] G. Pratt and M. Williamson, "Series elastic actuators," *Proc. IEEE/RSJ Int. Conf. Intelligent Robots and Systems*, vol. 1, p. 399, 1995.

[2] T. Morita, H. Iwata, and S. Sugano, "Development of human symbiotic robot: Wendy," in *Proc. IEEE Int. Conf. Robotics and Automation*, vol. 4, 1999, pp. 3183 –3188.

[3] M. Zinn, B. Roth, O. Khatib, and J. K. Salisbury, "A new actuation approach for human friendly robot design," *Int. J. Robotics Research*, vol. 23, no. 4-5, pp. 379–398, 2004.

[4] A. Albu-Schäffer, O. Eiberger, M. Grebenstein, S. Haddadin, C. Ott, T. Wimbock, S. Wolf, and G. Hirzinger, "Soft robotics: From torque feedback-controlled lightweight robots to intrinsically compliant systems," *IEEE Robot. Autom. Mag.*, vol. 15, no. 3, pp. 20 –30, Sep. 2008.

[5] S. Haddadin, A. Albu-Schäffer, and G. Hirzinger, "Requirements for safe robots: Measurements, analysis and new insights," *Int. J. Robotics Research*, vol. 28, no. 11-12, pp. 1507–1527, 2009.

[6] A. Bicchi and G. Tonietti, "Fast and "soft-arm" tactics," *IEEE Robot. Autom. Mag.*, vol. 11, no. 2, pp. 22 – 33, 2004.

[7] M. Van Damme, B. Vanderborght, B. Verrelst, R. Van Ham, F. Daerden, and D. Lefeber, "Proxy-based sliding mode control of a planar pneumatic manipulator," *Int. J. Robotics Research*, vol. 28, no. 2, pp. 266–284, 2009.

[8] T. Lens, J. Kunz, C. Trommer, A. Karguth, and O. von Stryk, "Biorobarm: A quickly deployable and intrinsically safe, light-weight robot arm for service robotics applications," in *Proc. 41st Int. Symp. Robotics / 6th German Conf. Robotics*, 2010.

[9] R. Schiavi, G. Grioli, S. Sen, and A. Bicchi, "VSA-II: a novel prototype of variable stiffness actuator for safe and performing robots interacting with humans," in *Proc. IEEE Int. Conf. Robotics and Automation*, 2008, pp. 2171–2176.

[10] R. Van Ham, T. Sugar, B. Vanderborght, K. Hollander, and D. Lefeber, "Compliant actuator designs," *IEEE Robot. Autom. Mag.*, vol. 16, no. 3, pp. 81–94, 2009.

[11] A. Albu-Schäffer, S. Wolf, O. Eiberger, S. Haddadin, F. Petit, and M. Chalon, "Dynamic modelling and control of variable stiffness actuators," in *Proc. IEEE Int. Conf. Robotics and Automation*, 2010, pp. 2155 –2162.

[12] D. Shin, I. Sardellitti, Y.-L. Park, O. Khatib, and M. Cutkosky, "Design and control of a bio-inspired human-friendly robot," *Int. J. Robotics Research*, vol. 29, no. 5, pp. 571–584, 2010.

[13] A. De Luca, B. Siciliano, and L. Zollo, "PD control with on-line gravity compensation for robots with elastic joints: Theory and experiments," *Automatica*, vol. 41, no. 10, pp. 1809 – 1819, 2005.

[14] B. Rooks, "The harmonious robot," *Industrial Robot: Int. J.*, vol. 33, pp. 125–130, 2006.

[15] A. Rost and A. Verl, "The quadhelix-drive - an improved rope actuator for robotic applications," in *Proc. IEEE Int. Conf. Robotics and Automation*, 2010, pp. 3254 –3259.

[16] T. Lens and O. von Stryk, "Investigation of safety in human-robot-interaction for a series elastic, tendon-driven robot arm," in *Proc. IEEE/RSJ Int. Conf. Intelligent Robots and Systems*, 2012.

[17] T. Lens, A. Karguth, and O. von Stryk, "Safety properties and collision behavior of robotic arms with elastic tendon actuation," in *Proc. 7th German Conf. Robotics*, 2012.

[18] B. Möhl, "Bionic robot arm with compliant actuators," in *Proc. Sensor Fusion and Decentralized Control in Robotic Systems III*, 2000, pp. 82–85.